Available online at www.sciencedirect.com
SCIENCE DIRECT
Journal of Catalysis 238 (2006) 321–329
JOURNAL OF CATALYSIS
www.elsevier.com/locate/jcat

Ozone promoted carbon monoxide oxidation on platinum/γ-alumina catalyst

Martin Petersson [a,b,c], David Jonsson [a,b], Hans Persson [a,c,d], Neil Cruise [a,e], Bengt Andersson [a,b,*]

[a] *Competence Centre for Catalysis, Chalmers University of Technology, SE-412 96 Göteborg, Sweden*
[b] *Chemical Reaction Engineering, Chalmers University of Technology, SE-412 96 Göteborg, Sweden*
[c] *Volvo Technology AB, Chalmers Science Park, SE-412 88 Göteborg, Sweden*
[d] *Department of Applied Physics, Chalmers University of Technology, SE-412 96 Göteborg, Sweden*
[e] *Perstorp Specialty Chemicals AB, Process and Catalyst, SE-284 80 Perstorp, Sweden*

Received 2 September 2005; revised 20 December 2005; accepted 3 January 2006

Available online 20 January 2006

Abstract

CO oxidation with oxygen and ozone–oxygen mixtures was studied over a platinum/alumina monolith catalyst. Temperature ramp experiments were combined with mean-field simulations to study the reaction mechanisms. In the absence of ozone, a slow CO oxidation reaction was observed at low temperatures. The rate of this slow reaction was proportional to the square root of the oxygen pressure and independent of the CO concentration. At higher temperatures, the three-step Langmuir–Hinshelwood reaction mechanism dominated the CO oxidations. When some of the oxygen was exchanged for ozone, rapid oxidation of CO by ozone was observed. The suggested explanation was an Eley–Rideal mechanism, in which colliding ozone reacts with adsorbed CO on the platinum surface. When this additional reaction step was included in the model, the simulation results indicated a reduction in the bulk CO pressure. The experimentally observed ozone promotion of CO oxidation was thus attributed to a decrease in CO surface self-poisoning.

Keywords: Catalysis; Low-temperature activity; CO oxidation; Ozone; Platinum; Pt/Al_2O_3; Mean-field modeling; Simulations

1. Introduction

The total oxidation of CO has been widely studied due to its importance in emission control. It is also a simple reaction between diatomic species and thus is well suited for theoretical studies. One of the first studies was presented by Langmuir [1], who suggested an Eley–Rideal type of reaction between adsorbed oxygen and colliding CO. Later works [2,3] showed that the reactions follow the three-step Langmuir–Hinshelwood reaction scheme under UHV conditions:

$$CO_g + S \rightleftarrows CO\text{–}S, \tag{1}$$

$$(O_2)_g + 2S \rightarrow 2O\text{–}S, \tag{2}$$

$$CO\text{–}S + O\text{–}S \rightarrow (CO_2)_g + 2S, \tag{3}$$

where the subscripts "g" refer to a gaseous species and S corresponds to a platinum site. The same reaction scheme has been shown to describe the reaction kinetics at atmospheric pressure if the lateral repulsion between nearest-neighbor CO–CO is explicitly taken into account [4].

Because CO and oxygen are competing for the same adsorption sites in the foregoing three-step Langmuir–Hinshelwood model, the reaction might be self-poisoned under some gas compositions. CO has a high initial sticking (in the order of 0.8) compared with the low initial oxygen sticking (usually reported as <0.1) [5]. Furthermore, oxygen requires two adjacent free sites, whereas CO requires just one site. As a result, the foregoing model predicts that the platinum surface will be almost completely CO-covered at low temperatures unless the oxygen content in the gas is much higher than the CO concentration. Therefore, virtually no reactions will occur unless the catalyst temperature is increased and the CO starts to desorb. CO desorption will provide access to the surface for oxygen, resulting in rapid oxidation of CO. The model thus predicts two stable states for CO oxidation, one state with high CO coverage and a low rate of oxidation and the other with high oxygen cover-

* Corresponding author. Fax: +46 31 772 3035.
E-mail address: bengta@chemeng.chalmers.se (B. Andersson).

0021-9517/$ – see front matter
doi:10.1016/j.jcat.2006.01.002

age and a high rate of oxidation. The bistable kinetics of the CO oxidation reaction has been studied previously [6–8].

Recently, an alternative reaction path for CO oxidation on platinum was suggested by Bourane and Bianchi [9–13]. According to this mechanism, the dissociative adsorption of oxygen occurs on a second site (denoted by S_2) without the competition of CO, followed by a consecutive reaction with adsorbed CO on the ordinary platinum sites (denoted by S_1). The heat of sorption for this oxygen species was found to be low (30 kJ/mol), which is why the specie was termed "weakly adsorbed" oxygen:

$$\mathrm{CO_g} + S_1 \rightleftarrows \mathrm{CO}\text{–}S_1, \tag{4}$$

$$(\mathrm{O_2})_g + S_2 \rightleftarrows 2\mathrm{O}\text{–}S_2, \tag{5}$$

$$\mathrm{CO}\text{–}S_1 + \mathrm{O}\text{–}S_2 \rightarrow (\mathrm{CO_2})_g + S_1 + S_2. \tag{6}$$

The adsorption equilibrium of the weakly adsorbed oxygen [Eq. (5)] explains the observed initial reaction order of 1/2 for oxygen in CO excess [11], where the conventional three-step Langmuir–Hinshelwood model would predict a reaction order of zero for oxygen. At catalyst ignition, Bourane and Bianchi suggested that the reduced platinum surface is rapidly converted into an oxygen-covered surface with different kinetics, thus explaining the observed bistable kinetics of CO oxidation [13].

The self-poisoning of CO oxidation has been well established in many industrial applications. Several techniques have been evaluated for decreasing CO blockage of the platinum surface. The techniques evaluated thus far include the addition of various promoters, which will allow oxygen to spillover to the reactive sites [14–18] or create new adsorption sites for oxygen at the noble metal surface [19,20]. Other approaches include optimal positioning of the noble metal [21], periodic variations in exhaust gas composition [22,23], and photo-enhanced oxidation [24].

One alternative approach suggested in the patent literature is to add ozone to the exhaust gas [25]. CO oxidation in the presence of ozone has been studied over MnO_2 [26], CeO_2 [27], Co_2O_3 [28], and Au/Fe_2O_3 [29]. It has also been used to promote the total oxidation of volatile organic compounds over noble metal catalysts [30]. As far as we know, however, the present study is the first scientific study of CO oxidation over supported platinum catalysts in the presence of ozone.

In the current study, oxidation of CO was studied in oxygen and in ozone–oxygen mixtures to investigate the promotional effect of ozone on the CO oxidation reaction. To study the reaction mechanisms of CO oxidation with oxygen and with ozone, flow reactor experiments were combined with mean-field modeling. In the model, a conventional three-step Langmuir–Hinshelwood mechanism for CO oxidation in oxygen was combined with the noncompeting model of Bourane and Bianchi to describe the observed CO oxidation even at almost complete CO coverage. Reaction steps for ozone reaction with CO and ozone decomposition are also included.

Table 1
Pt/Al_2O_3 monolith sample properties

Property	Value	Unit
Diameter	20	mm
Length	40	mm
Sample weight	6.68	g
Washcoat weight	1.12	g
Platinum content	1.0	wt%
BET surface area	22.5	m^2/g
Noble metal dispersion	10.7	%

2. Experimental

2.1. Catalyst preparation and characterization

A cylindrical core (diameter, 20 mm; length, 50 mm) was cut out of a commercial corderite monolith (Corning Glass; 400 cpsi, 6.5-mil wall thickness). This core was coated with γ-alumina (16.8 wt%) and calcined at 873 K for 1 h in air. It was then impregnated with a platinum ammonium nitrate solution (Johnson Matthey) to achieve a platinum content of 1 wt% of the washcoat, using the incipient wetness impregnation method, and finally calcined at 823 K for 90 min in air.

This catalyst sample was trimmed off to 40 mm. The excess material was used to analyze total surface area and noble metal dispersion using a Multisorb ASAP 2010 instrument (Micromeretics). The total surface area was determined from five nitrogen adsorption–desorption measurements at relative nitrogen pressures of 0.06–0.21, assuming a 0.162-nm^2 cross-sectional area of the nitrogen adsorbate. The noble metal dispersion was determined from the irreversible CO adsorption at 307 K. The irreversible CO adsorption was determined as the difference between two repeated CO adsorption measurements at five different CO pressures. Each surface platinum atom was assumed to adsorb 0.7 CO molecules [31]. The basic characteristics of this catalyst are given in Table 1.

2.2. Flow reactor experiments

CO oxidation experiments were conducted in a vertically-mounted metal tube reactor. The reactor tube had a diameter of 20 mm, but had a flow restrictor that decreases the effective sample diameter to 17.5 mm. The gas entering the reactor was heated by a capillary preheater, and the reactor wall was heated by metallic heating coils. The temperature was measured by thermocouples before and after the catalyst and at the reactor wall; separate temperature control units were used to regulate the temperature in the capillary preheater and the tube reactor. A sintered quartz frits was mounted between the preheater and the catalyst sample to distribute the gas evenly over the reactor cross-section.

Three separate mass flow controllers (Brooks Instrument models 5850E and 5850S) were used to mix the reactor feed stream from argon (AGA gas, 99.996%), CO (AGA gas, 99%), and oxygen (AGA gas, 99.95%). The oxygen gas stream was flown through a high-voltage discharge ozone generator (Thermo Electron model 100B) before the gases was mixed.

During the experiments without ozone, the ozone generator was turned off. All tubing between the ozone generator and the preheater was made of Teflon, and the amount of tubing was minimized to minimize ozone decomposition. The CO concentration in the gas leaving the reactor was determined with an infrared analyzer (Thermo Environmental Instruments model 48C).

CO conversion was determined under constant heating ramps from 350 to 555 K at 10 K/min. In all experiments, the overall gas flow was 3207 mL/min, corresponding to a space velocity of 20,000 h^{-1}. The CO concentration was varied between 0.1 and 0.5%, and the oxygen concentration was varied between 1 and 5%.

To determine the ozone concentration reaching the catalyst, empty reactor measurements were conducted. The ozone concentration was recorded using a UV analyzer (Dasibi Enviromental model 1000-AH). Due to the limited maximum measurement range of the UV analyzer, the sample gas was diluted with air at dilution ratios of 25.9 and 44.7 to give analyzable concentrations. These experiments were then repeated with CO present in the feed, to determine whether the homogeneous gas-phase reaction between ozone and CO could affect the results. Furthermore, an alumina-coated monolith sample, prepared as above with no impregnation of noble metal, was used to determine whether any reaction occurred on the support.

3. Results and discussion

3.1. Measured ozone concentration and blank sample tests

Fig. 1 shows the concentration of ozone in the gas leaving the empty reactor. The ozone concentration was found to be weakly dependent on the oxygen concentration. Measurements in the gas stream entering the reactor indicated that a minor part of the ozone was decomposed in the reactor at 323 K (<1% conversion). At higher temperatures, ozone decomposition in the reactor became significant. No ozone was detected from the empty reactor above 530 K.

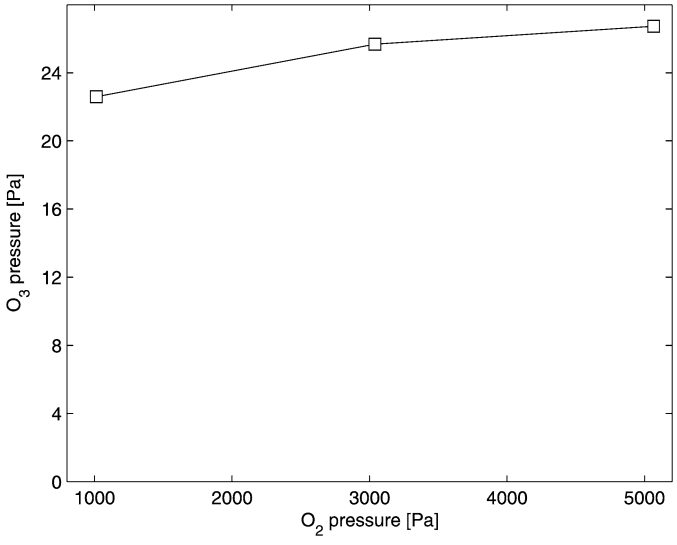

Fig. 1. Measured ozone concentration at 323 K with varying oxygen concentrations.

To determine the CO oxidation in any competing reactions, measurements were conducted over a γ-alumina-coated sample with and without ozone. The measurements were conducted with 0.1 CO and 5% oxygen at constant temperature points. Without ozone, no CO oxidation could be detected below 425 K, whereas up to 8% conversion could be detected at 435 K. In the presence of ozone, some CO oxidation could be detected at 375 K and almost 17% conversion was detected at 435 K.

3.2. Measured carbon monoxide oxidation during heating ramps

The temperature ramp experiments are presented in Figs. 2A–C. The oxidation of CO by oxygen was increased by increased oxygen concentrations and by decreased CO concentrations. The observed dependence of the CO concentration indicates that the oxidation reaction was self-poisoned by CO.

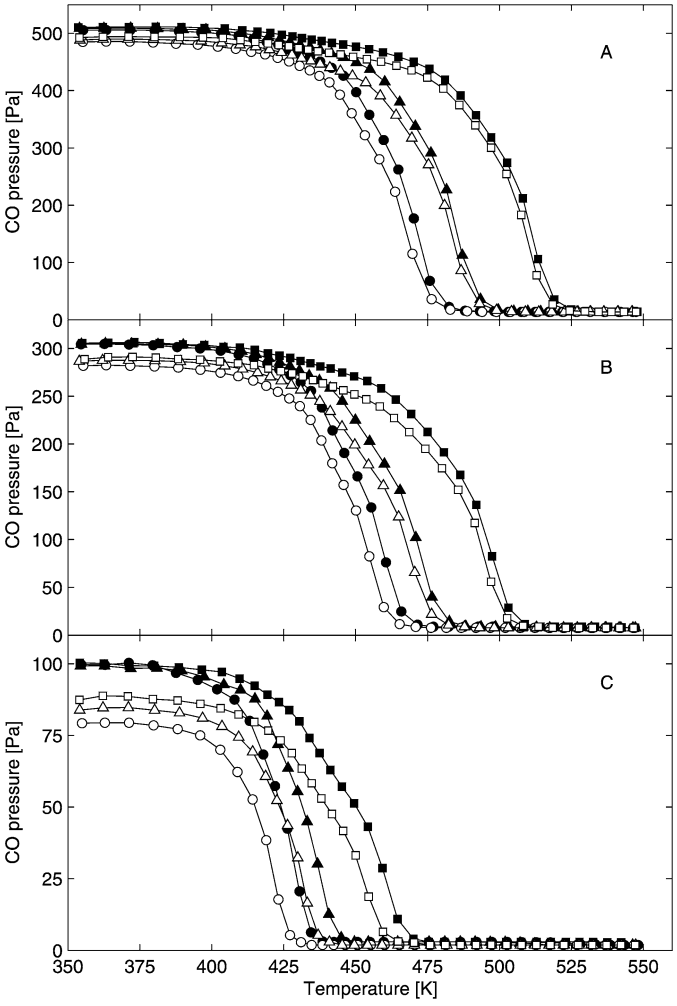

Fig. 2. Measured CO concentrations during ramp experiments (10 K/min) with (A) 0.5, (B) 0.3, and (C) 0.1% CO. Squares, triangles and circles corresponds to 1, 3, and 5% oxygen. Empty and filled symbols represent measurements with and without ozone, respectively.

It was also found that ozone has a promotional effect on the CO oxidation. This effect was more pronounced at low CO concentrations, but seemed to be independent of the oxygen concentration. Finally, at temperatures well below catalyst light off, some CO oxidation was found in the presence of ozone. This low-temperature reaction was increased with increasing oxygen concentration and decreasing CO concentration.

Comparing these results with the blank alumina oxidation experiments presented in Section 3.1 shows that the rate of CO oxidation on the blank sample was small. At 425 K with 0.1% CO, 5% oxygen, and no ozone, the platinum-coated sample had about 70% conversion, compared with the 8% measured with the blank sample. The same findings were seen in the presence of ozone, with complete oxidation measured over the platinum-containing sample and only 17% conversion over the blank sample.

One important finding shown in Figs. 2A–C is the initial slow decrease in CO concentration in the absence of ozone. For the experiment with 0.5 CO and 5% oxygen (Fig. 2A, black squares), CO concentration began to decline around 400 K, but catalyst light-off did not occur until the inlet temperature exceeded 475 K. A similar slow initial CO oxidation reaction was observed for all the other temperature ramp experiments both with and without ozone.

To study this slow reaction in detail, the CO oxidation rate was calculated from the low conversion points (<20% conversion) without ozone. The low conversion made it possible to approximate the reactor as one continuous stirred tank. Quasi-steady state was assumed, because the observed reaction rate was approximately 0.5/s and the collision rate of CO and oxygen on a Pt site was on the order of 10^5–10^7/s for the current inlet gas pressures. The results from these calculations are given in Fig. 3A. It was found that rate of oxidation was determined by the oxygen concentration and that the rate was independent of the CO concentration. Investigating the oxygen concentration dependence, the rate was found to be proportional to the square root of the oxygen pressure, as shown in Fig. 3B. This slow CO oxidation thus appears to follow the model suggested by Bourane and Bianchi, which is described in Eqs. (4)–(6).

3.3. Model for CO oxidation with oxygen

The CO oxidation reaction was described by the conventional three-step Langmuir–Hinshelwood mechanism, combined with the noncompeting mechanism suggested by Bourane and Bianchi:

$$\mathrm{CO_g} + S_1 \underset{r_2}{\overset{r_1}{\rightleftarrows}} \mathrm{CO}\text{–}S_1, \tag{7}$$

$$(\mathrm{O_2})_\mathrm{g} + 2S_1 \xrightarrow{r_3} 2\mathrm{O}\text{–}S_1, \tag{8}$$

$$\mathrm{CO}\text{–}S_1 + \mathrm{O}\text{–}S_1 \xrightarrow{r_4} (\mathrm{CO_2})_\mathrm{g} + 2S_1, \tag{9}$$

$$(\mathrm{O_2})_\mathrm{g} + S_2 \underset{r_6}{\overset{r_5}{\rightleftarrows}} 2\mathrm{O}\text{–}S_2, \tag{10}$$

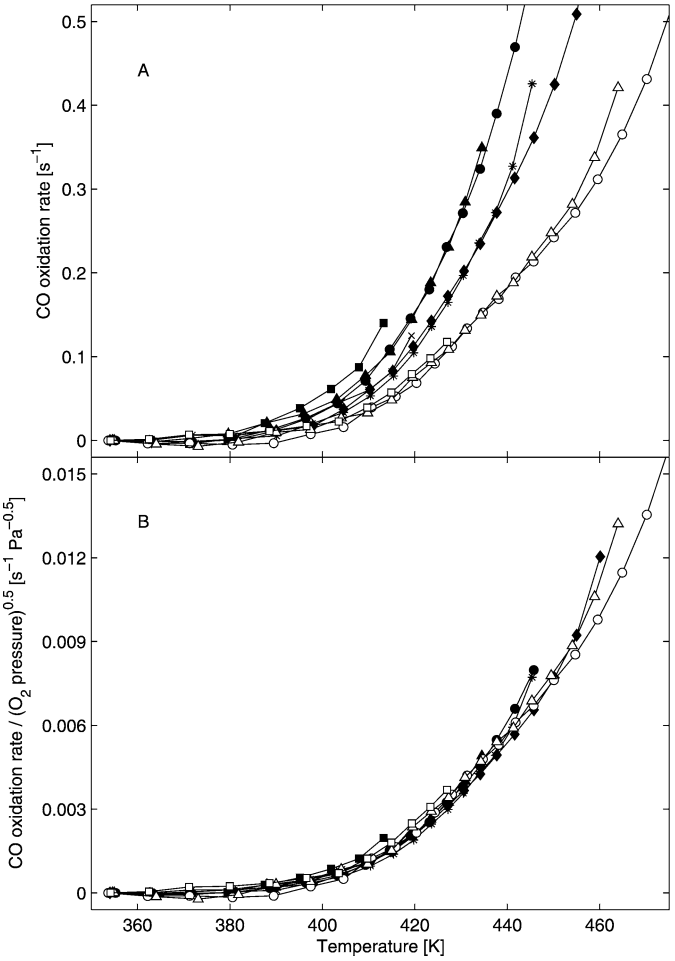

Fig. 3. (A) Approximate CO oxidation rate during ramp experiments (10 K/min) at conversions less than 20%. Filled squares corresponds to 0.1% CO and 5% oxygen, filled triangles 0.3% CO and 5% oxygen, filled circles 0.5% CO and 5% oxygen, cross 0.1% CO and 3% oxygen, stars 0.3% CO and 3% oxygen, filled diamonds 0.5% CO and 3% oxygen, open squares 0.1% CO and 1% oxygen, open triangles 0.3% CO and 1% oxygen, and open circles 0.5% CO and 1% oxygen. (B) Approximate CO oxidation rate divided with the square root of the inlet oxygen concentration during ramp experiments (10 K/min) at conversions less than 20%. Annotations as above.

$$\mathrm{CO}\text{–}S_1 + \mathrm{O}\text{–}S_2 \xrightarrow{r_7} (\mathrm{CO_2})_\mathrm{g} + S_1 + S_2, \tag{11}$$

where S_1 and S_2 correspond to two different platinum sites. The three-step Langmuir–Hinshelwood mechanism [Eqs. (7)–(9)] was used to explain the CO self-poisoning observed at elevated conversions, whereas the model proposed by Bourane and Bianchi [Eqs. (7) and (10)–(11)] was essential to describe the slow CO oxidation discussed in Section 3.2.

The surface coverages of reactants and bulk gas concentrations were expressed according to the standard mean-field model. The rate expressions and parameter values used in the simulation are given in Table 2. The collision rate of CO and oxygen on site S_1 was calculated according to kinetic gas theory with a Pt site size of 8 Å^2 [32]. The sticking coefficient for oxygen on site S_1 was set proportional to P_{00}, that is, the probability that a pair of nearest neighbor sites is vacant. This probability was taken from the quasi-chemical approximation [33] with a CO–CO lateral interaction of $E_{\mathrm{CO}}^{\mathrm{rep}}$ (see Table 2)

Table 2
Kinetic parameters for simulation of CO oxidation on Pt/Al_2O_3. All rates are expressed per site S_1, except r_9 which is expressed per weight of washcoat. Parameters with confidence intervals were fitted in the current study

Process and rate expression	Parameter	Value	95% conf.	Unit
CO adsorption on site S_1:	$s^{(0)}_{CO}$	0.84	Ref. [6]	
$r_1 = s^{(0)}_{CO} \cdot (1-\theta^2_{CO}) \cdot k^a_{CO} p_{CO,w}$				
CO desorption from site S_1:	ν^d_{CO}	1.25×10^{15}	Ref. [6]	s^{-1}
$r_2 = \nu^d_{CO} \exp\left(-\left(E^{d,0}_{CO}(1-\alpha\theta_{CO})\right)/RT\right) \cdot \theta_{CO}$	$E^{d,0}_{CO}$	180	Ref. [37]	kJ/mol
	α	0.5254	±0.0011	
Oxygen adsorption on site S_1:	$s^{(0)}_{O_2,S_1}$	0.02	Ref. [30]	
$r_3 = s^{(0)}_{O_2,S_1} P_{00}\left(\theta_{CO}, \theta_{O,S_1}, E^{rep}_{CO}\right) \cdot k^a_{O_2,S_1} p_{O_2,w}$	E^{rep}_{CO}	26.34	±0.11	kJ/mol
CO reacting with oxygen from site S_1:	ν_4	1.65×10^{14}	Ref. [6]	s^{-1}
$r_4 = \nu_4 \exp\left(-E^0_4(1-\beta\theta_{CO})/RT\right) \cdot \theta_{CO}\theta_{O,S_1}$	$E^{r1,0}$	100.9	Ref. [6]	kJ/mol
	β	0.5	Ref. [30]	
Oxygen equilibrium on site S_2:	$E^d_{O_2,S_2}$	30	Ref. [9]	kJ/mol
$K_{O_2,S_2} = \frac{(h_{plank})^3}{k_B(2\pi m_{O_2} k_B)^{3/2}} \frac{1}{T^{5/2}} \exp\left(\frac{E^d_{O_2,S_2}}{RT}\right)$				
Oxygen desorption from site S_2:				
$r_6 = (k_B T/h_{plank}) \exp\left(-E^d_{O_2,S_2}/RT\right) \cdot \theta^2_{O,S_2}$				
CO reacting with oxygen from site S_2:	E_7	67.66	±0.36	kJ/mol
$r_7 = (k_B T/h_{plank}) \exp(-E_7/RT) \cdot \theta_{CO} \cdot (n_{S_2}/n_{S_1}) \cdot \theta_{O,S_2}$	n_{S_2}	5.49×10^{-4}	$\pm 3.0 \times 10^{-5}$	mol/m^3
CO reacting with ozone				
$r_8 = k^a_{O_3,S_1} p_{O_3,w} \theta_{CO}$				
O_3 decomposition on site S_3:	ν_9	1.95	±0.16	mol/(Pa kg s)
$r_9 = \nu_9 p_{O_3,w}$				

and all other lateral interactions assumed to be negligible, as described previously [34]. The rate constant for adsorption of oxygen on site S_2 was calculated from the adsorption equilibrium constant and the rate constant for desorption.

The transient response of the monolith catalyst was modeled as a single monolith channel comprising of 30 continuous stirred tank reactors. Mass transport between the gas bulk and the catalyst wall was described with the film model [35]. The mass transfer coefficient was calculated from a Sherwood number for monolith channels [36] with an asymptotic value of 2.98 [37]. The diffusivities and viscosities were calculated according to the Chapman–Enskog equations [35]. Pore transport limitations were not included in the model, because Weisz modulus calculations indicated that these limitations would not significantly affect the results. The tank series model for the monolith was coupled to a model describing the response time of the CO instrument. This CO instrument model consisted of one time lag and one continuous stirred tank. The time lag (15 s) and tank volume (1.49 ± 0.03 dm^3) were fitted to step-change experiments at low temperature (not shown), using lsqnonlin in Matlab.

The heat transfer coefficient, used in the bulk gas mass balance, was determined by setting the Nusselt number equal to the Sherwood number. The heat conductivity of the gas was determined using the Chapman–Enskog equation [35]. The heat balance for the catalyst wall included heat convection from the bulk gas, heat conduction between neighboring tanks, radiation heat transfer from reactor inlet and outlet to each tank, radial heat losses, and CO oxidation enthalpy. Radiation heat transfer between the tanks in the reactor was neglected because it was low compared with heat conduction in the monolith. A slight drop in catalyst outlet temperature was observed at high temperatures, attributed to the radiation heat transfer between the monolith and the reactor lid. The finite area view factors for this heat transfer were taken from Ref. [38]. The reactor lid was modeled as one thermal mass that interacted with the monolith only through radiation heat transfer. The heat capacity of the lid was fitted to 0.432 ± 0.021 J/K. The radiation heat transfer was low compared with the conducted heat transfer to the reactor wall. The radial heat loss coefficient was fitted to 13.08 ± 0.66 $W/(m^2\,K)$. The heat conductivity and specific heat capacity of the monolith [39] and the reaction enthalpy for CO oxidation [34] were as reported previously. The kinetic and heat transfer parameters were fitted to the measured CO instrument signal and the catalyst outlet temperature from the ramp experiments without ozone, using lsqnonlin in Matlab.

3.4. Simulation results for CO oxidation with oxygen

The modeled instrument signals are compared with the measured signal in Fig. 4. Good agreements between the results were found for all CO and oxygen concentration combinations. If the model suggested by Bourane and Bianchi is removed from the CO oxidation model, the deviation between the simulation and the measured results becomes significant before catalyst light-off, as shown in Fig. 5.

The detailed simulation results for the model with the reaction path suggested by Bourane and Bianchi for 0.1% CO and 5% oxygen and 0.5% CO and 1% oxygen are shown in Fig. 6. At low temperatures, the coverage of CO on site S_1 was close to unity, resulting in very low oxygen coverage at site S_1

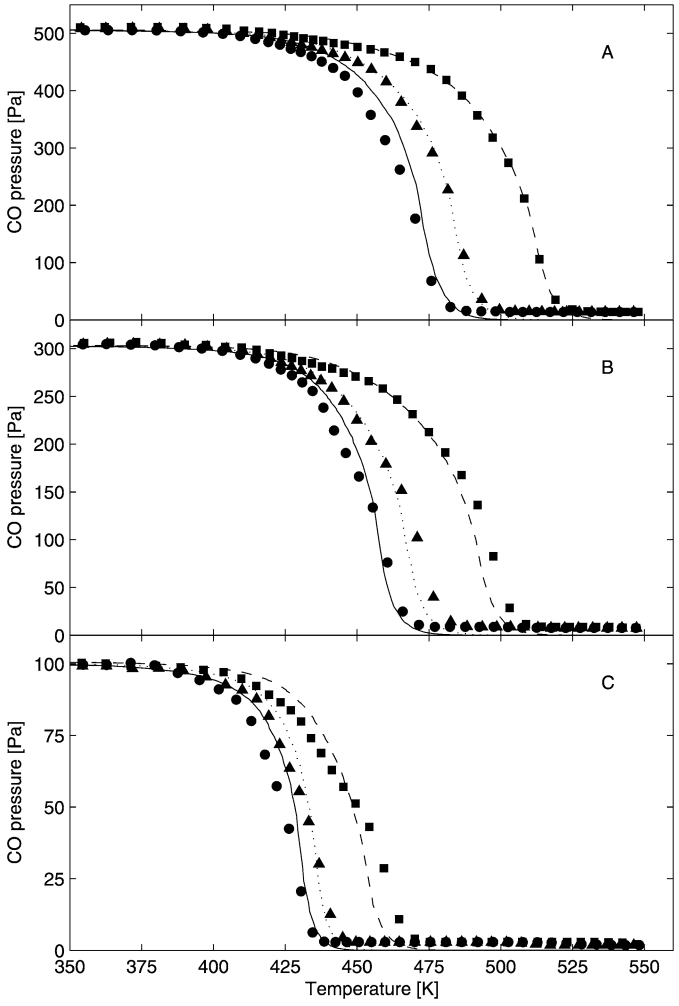

Fig. 4. Measured and simulated CO instrument signals during ramp experiments (10 K/min) without ozone and with (A) 0.5, (B) 0.3, and (C) 0.1% CO. Simulations include the model proposed by Bourane and Bianchi. Squares, triangles and circles corresponds to measurements with 1, 3, and 5% oxygen. Dashed, dotted and solid lines correspond to simulations with 1, 3 and 5% oxygen.

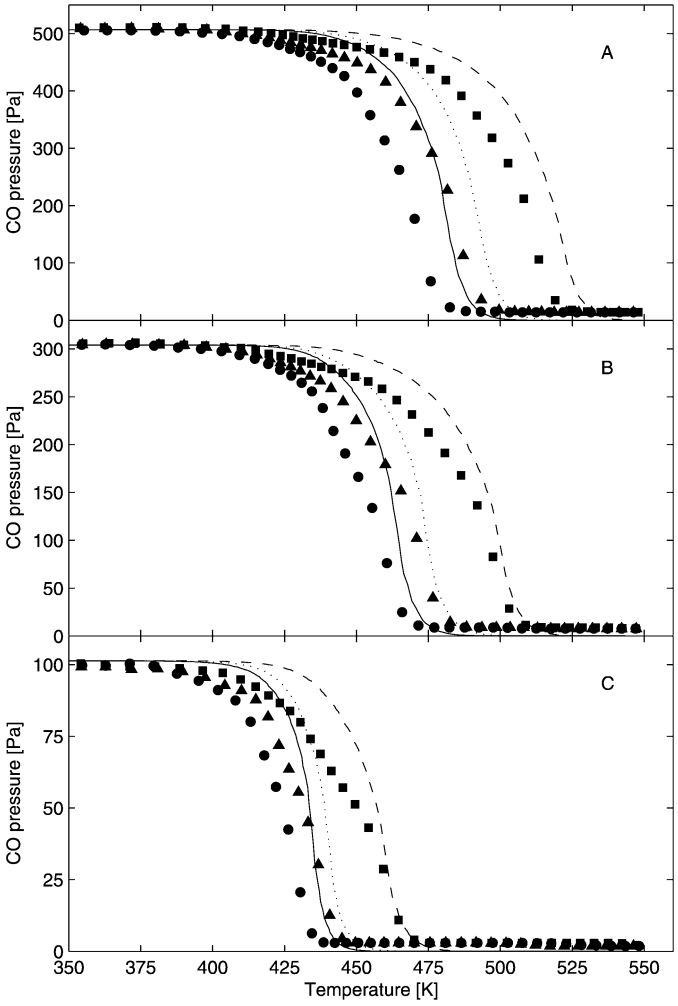

Fig. 5. Measured and simulated CO instrument signals without the model proposed by Bourane and Bianchi during ramp experiments (10 K/min) without ozone and with (A) 0.5, (B) 0.3, and (C) 0.1% CO. The parameters from Table 2 were used in the simulation, but with the number of S_2 sites (n_{S_2}) set to zero. Squares, triangles and circles corresponds to measurements with 1, 3 and 5% oxygen. Dashed, dotted and solid lines correspond to simulations with 1, 3, and 5% oxygen.

and consequently a low rate for the surface reaction on site S_1 [Eq. (9)]. The overall CO oxidation rate was instead controlled by the reaction with oxygen on site S_2 [Eqs. (10) and (11)]. The slow rate of this surface reaction [Eq. (11)] resulted in oxygen coverage close to equilibrium on site S_2. This coverage was thus proportional to the square root of the oxygen pressure, as is seen when comparing Figs. 6G and H. As the temperature was increased, CO adsorbed on S_1 sites began to desorb, causing the rate of oxygen adsorption on S_1 sites to increase and the rate of reaction between CO and oxygen on site S_1 to become increasingly important. When the CO coverage decreased below a certain threshold level, a rapid transformation from a CO-covered surface to an oxygen-covered surface occurred. The rapid transformation shows that the CO oxidation reaction was controlled by the adsorption/desorption processes [Eqs. (7) and (8)] rather than surface kinetics [Eq. (9)]. The threshold level was dependent on the CO and oxygen concentrations, and the transformation started from the end of the catalyst and migrated toward the inlet. At high temperatures, the bulk gas concentration leveled out to a finite level in the first couple of tanks, indicating that the rate of oxidation became external mass transfer-limited.

The three-step Langmuir–Hinshelwood part of the model above is closely related to the model presented by Rinnemo et al. [34]. In the present model, the desorption energy of CO at low coverage was higher than in the model suggested by Rinnemo (180 kJ/mol compared with 146 kJ/mol). The reported CO desorption energies for platinum single crystals with low CO coverage range from 138 [2] to 180 kJ/mol [40], with reports of energies up to 220 kJ/mol for supported platinum/alumina catalysts [41]. Previous CO modeling studies performed by our group found CO desorption energies of 180 kJ/mol [21,42]. The increase in low-coverage CO desorption energy also required a change in CO cover dependence of the CO desorption energy and CO–CO lateral interaction.

The oxygen adsorption and reaction model on site S_2 was based on the model of Bourane and Bianchi. To combine it with the three-step Langmuir–Hinshelwood model, the model

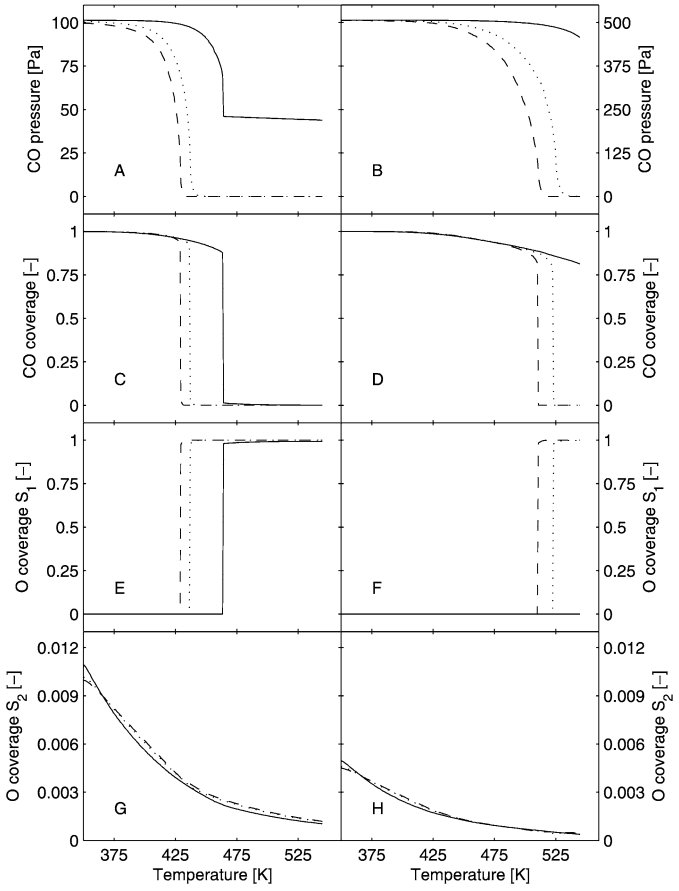

Fig. 6. Results from simulations of temperature ramps (10 K/min) with 0.1% CO and 5% oxygen (A, C, E, and G), and with 0.5% CO and 1% oxygen (B, D, F, and H). Simulations include the model proposed by Bourane and Bianchi. A and B show bulk gas pressure of CO, C and D show CO coverage, E and F show O coverage on site S_1, and G and H show O coverage on site S_2. Solid, dotted and dashed lines correspond to tank 1, 15, and 30 respectively.

of Bourane and Bianchi was reformulated to explicitly account for the transient coverage of oxygen on site S_2. This required that the number of S_2 sites be determined. The number of S_2 sites (n_{S_2}) was found to account for 0.16% of the total number of surface platinum sites. The low number of S_2 sites suggests that these sites were edge, corner, or defect sites on the platinum crystals. The activation energy of the surface reaction was within the range determined by Bourane and Bianchi [9].

3.5. Model for CO oxidation with ozone

Based on the results presented in Figs. 2A–C, addition of ozone to the reaction caused a low-temperature CO oxidation reaction on the platinum sites. The ratio of oxidized CO to feed ozone concentration at low temperature was between 0.5 and 1, suggesting that the dominating reaction between CO and ozone occurred with a stoichiometric coefficient of 1. Furthermore, the foregoing simulations show that the platinum surface was almost completely covered with CO at these temperatures, which is why the most likely explanation for the observed reaction is an Eley–Rideal reaction, in which adsorbed CO reacts with colliding ozone molecules. The alternative explanation that ozone dissociates and reacts with adsorbed CO is less likely because of the low number of free platinum sites and the observation that the apparent stoichiometric coefficient was <1.

No ozone decomposition occurred over the empty reactor at 323 K, but significant ozone conversion was detected at elevated temperatures. Comparing the residence time in the reactor with the lifetime of ozone in air at different temperatures [43] demonstrated that the observed ozone conversion can be attributed to a homogeneous gas-phase reaction. But this reaction was negligible compared with the heterogeneous reaction on alumina, because no ozone could be detected over an alumina-coated monolith, indicating that ozone decomposition was rapid even on the alumina surface. Therefore, the measured outlet ozone concentration presented in Fig. 1 was used as the ozone inlet concentration in the ozone simulations.

To model the observed reactions, it was thus sufficient to complement the reaction mechanism for CO oxidation in the absence of ozone [Eqs. (7)–(11)] with one Eley–Rideal reaction between ozone and adsorbed CO and one ozone decomposition step on the alumina surface:

$$(O_3)_g + CO\text{–}S_1 \xrightarrow{r_8} (O_2)_g + (CO_2)_g + S_1, \tag{12}$$

$$(O_3)_g \xrightarrow[S_3]{r_9} \frac{3}{2}(O_2)_g, \tag{13}$$

where S_3 corresponds to a site on the alumina wash coat. No ozone decomposition reaction on platinum was included, because of the low number of free platinum sites observed in the CO oxidation calculations with oxygen, which is why this reaction was assumed to be negligible. The rate expressions for the two reactions are given in Table 2. The rate constant for ozone colliding and reacting with adsorbed CO [Eq. (12)] was calculated according to kinetic gas theory, with a reaction probability of 1. The ozone decomposition rate constant (ν_9) was fitted to the CO instrument signal during the ramp experiments with ozone, using lsqnonlin in Matlab. It was assumed that the decomposition of ozone on site S_3 [Eq. (13)] was not activated. The decomposition rate was expressed per mass of wash coat rather than per site, because the site density was not yet established. The value of ν_9 is given in Table 2. The ozone reactions were implemented in the mass and heat transfer model from Section 3.4. The Lennard–Jones parameters needed to determine ozone diffusivity were estimated from the critical temperature and volume of ozone [35]. The reaction enthalpy of ozone was as specified in the literature [44].

3.6. Simulation results for CO oxidation with oxygen–ozone mixtures

Fig. 7 shows a comparison between the simulated CO instrument signals and the measured signals. The agreement between the results was good for all CO and oxygen concentration combinations. Weizs modulus calculations indicate that pore transport limitations will be negligible for all reactants. The detailed simulation results for 0.1% CO and 5% oxygen and ozone, and for 0.5% CO and 1% oxygen and ozone are shown

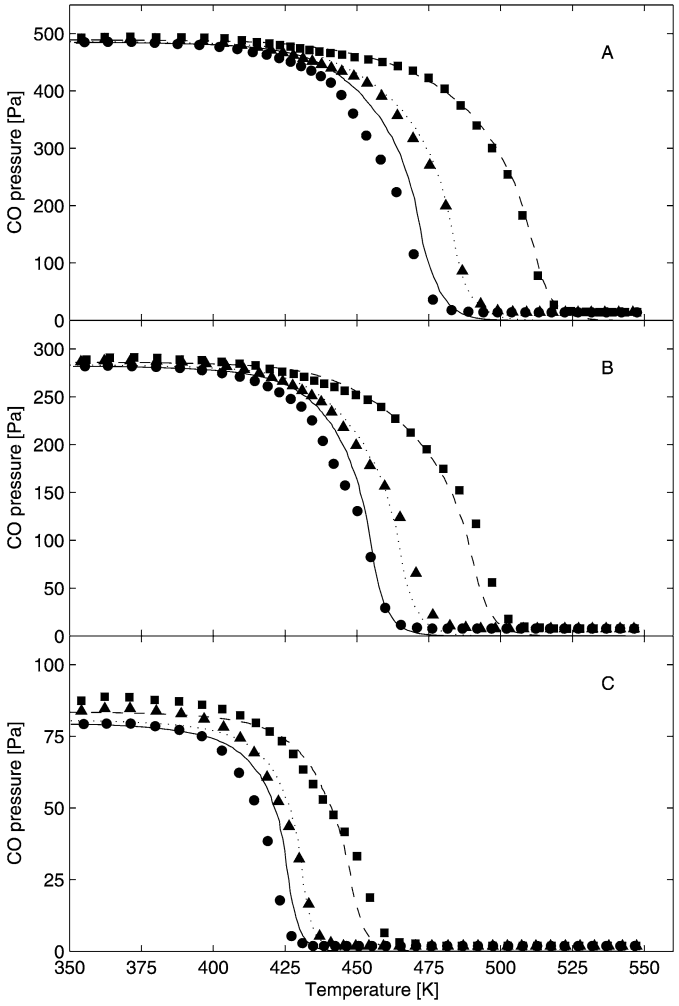

Fig. 7. Measured and simulated CO instrument signals during ramp experiments (10 K/min) with ozone and with (A) 0.5, (B) 0.3, and (C) 0.1% CO. Squares, triangles and circles corresponds to measurements with 1, 3, and 5% oxygen. Dashed, dotted and solid lines correspond to simulations with 1, 3, and 5% oxygen.

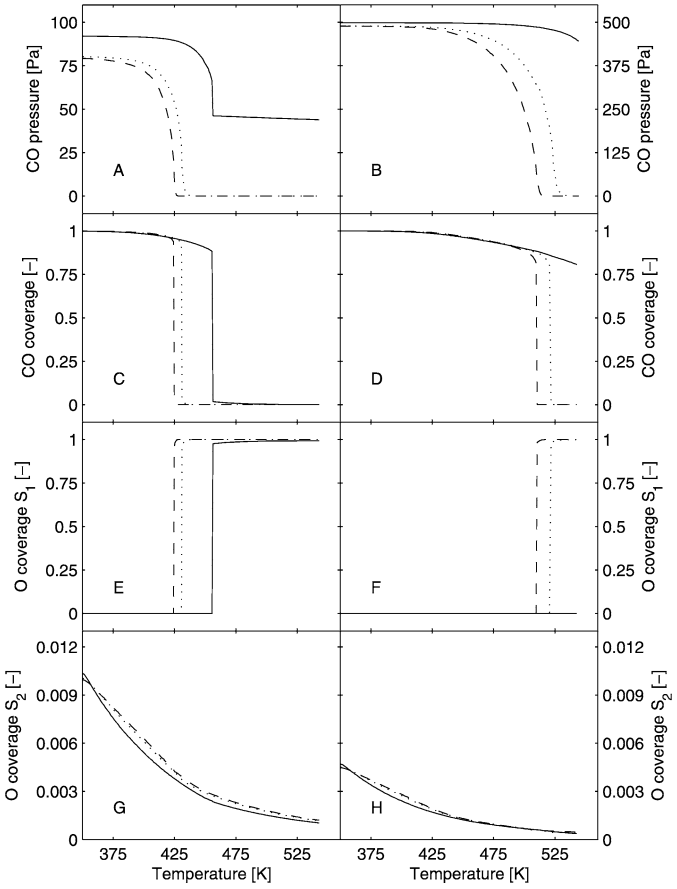

Fig. 8. Results from simulations of temperature ramps (10 K/min) with 0.1% CO, 5% oxygen and ozone (A, C, E, and G), and with 0.5% CO, 1% oxygen and ozone (B, D, F, and H). A and B show bulk gas pressure of CO, C and D show CO coverage, E and F show O coverage on site S_1, and G and H show O coverage on site S_2. Solid, dotted, and dashed lines correspond to tank 1, 15, and 30 respectively.

in Fig. 8. The results shown in Figs. 8A and B indicate that the reaction between CO and ozone occurred primarily in the first couple of tanks, and that 90% of the ozone was decomposed after 8 mm. While the surface was CO covered, the dominating reaction path for ozone was the reaction with CO on site S_1. Before light-off, 71–76% of the ozone was decomposed through this reaction. The very rapid reaction between CO and ozone makes it difficult to study the kinetic parameters for this reaction. Even though we have achieved good agreement with the experiments solely by adjusting the rate of ozone decomposition, we would suggest that future studies of the CO + ozone reaction be conducted at temperatures well below room temperature. This is beyond the scope of the current study, however.

The CO coverage (Figs. 8C and D) was not significantly affected by the reaction between CO and ozone at low temperatures. The S_1 sites that were emptied in that reaction thus were quickly CO-covered once again. But the reaction did result in a decrease in bulk CO pressure, which led to a decrease in CO self-poisoning and consequently a higher rate for the reactions with oxygen. This conclusion is supported by the observation that the transformation from CO-covered surfaces to oxygen-covered surfaces began at the outlet of the catalyst and migrated toward the catalyst inlet. Nonetheless, the decrease in CO pressure resulted in a somewhat earlier catalyst light-off compared with the experiments without ozone, and the overall oxidation reaction thus can be considered ozone-promoted.

The high rate of reaction between CO and ozone suggests that it is possible to achieve complete CO removal at room temperature, given a sufficient supply of ozone. It should also be possible to use ozone to force a catalyst from the CO-covered surfaces to the oxygen-covered surfaces under bistable reaction conditions, even though that effect was not observed in the current study. One drawback of this CO abatement technique is the high energy consumption associated with ozone production. It may be possible to reduce the ozone requirement by pulsing the ozone supply. It has been shown that catalyst light-off will occur at lower average oxygen to CO ratios under oxygen pulses compared with stationary oxygen concentrations [23], and we predict a similar effect for the current system.

4. Conclusion

The findings of our study of the reaction mechanism of CO oxidation over a platinum/alumina monolith catalyst comparing temperature ramp experiments with mean-field simulations can be summarized as follows:

1. The three-step Langmuir–Hinshelwood model, with lateral CO–CO interactions explicitly included via the quasi-chemical approximation, was not sufficient to describe the observed slow CO oxidation at low temperatures.
2. The rate of oxidation for this reaction was found to be proportional to the square root of the oxygen concentration and independent of the CO concentration, thus showing the same reaction order as reported by Bourane and Bianchi [9–13].
3. As the temperature was increased, the dominating oxidation process was changed to the conventional three-step Langmuir–Hinshelwood reaction.
4. The experimental results were well fitted when using a simulation model that combined the Bourane and Bianchi mechanism with the three-step Langmuir–Hinshelwood mechanism.
5. Exchanging some of the oxygen for ozone, a rapid reaction between CO and ozone was observed on the platinum surface. To model this reaction, the CO oxidation model described above was combined with an Eley–Rideal reaction between ozone and adsorbed CO and an ozone decomposition step on the alumina surface. The simulation results indicated that ozone addition caused a reduction in bulk CO concentration, and consequently a decrease in CO self-poisoning and a lower catalyst light-off temperature. Ozone was thus found to have a promotional effect on the CO oxidation reaction.

Acknowledgments

The authors thank Dr. Per-Anders Carlsson for providing the original Matlab simulation code. Financial support was provided by the Swedish Research Council for Engineering Sciences (grant 285-99-291). The work reported herein was conducted at the Competence Centre for Catalysis, which is supported by the Swedish Energy Agency and member companies: AB Volvo, Saab Automobile AB, Johnson Matthey CSD, Perstorp AB, AVL–MTC AB, Albemarle Catalysts, and the Swedish Space Administration.

References

[1] I. Langmuir, Trans. Faraday Soc. 17 (1922) 621.
[2] T. Engel, G. Ertl, Adv. Catal. 28 (1979) 1.
[3] G. Ertl, Adv. Catal. 37 (1990) 213.
[4] V.P. Zhdanov, B. Kasemo, Appl. Surf. Sci. 74 (1994) 147.
[5] V.P. Zhdanov, B. Kasemo, Surf. Sci. Rep. 39 (2000) 25.
[6] M. Bär, Ch. Zülike, M. Eiswirth, G. Ertl, J. Chem. Phys. 96 (1992) 8595.
[7] P.A. Carlsson, V.P. Zhdanov, B. Kasemo, Appl. Surf. Sci. 239 (2005) 424.
[8] M. Berdau, G.G. Yelenin, A. Karpowicz, M. Ehsasi, K. Christmann, J.H. Block, J. Chem. Phys. 110 (1999) 11551.
[9] A. Bourane, D. Bianchi, J. Catal. 202 (2001) 34.
[10] A. Bourane, D. Bianchi, J. Catal. 209 (2002) 114.
[11] A. Bourane, D. Bianchi, J. Catal. 209 (2002) 126.
[12] A. Bourane, D. Bianchi, J. Catal. 220 (2003) 3.
[13] A. Bourane, D. Bianchi, J. Catal. 222 (2004) 499.
[14] A. Holmgren, D. Duprez, B. Andersson, J. Catal. 182 (1999) 441.
[15] S. Johansson, L. Östlund, B. Kasemo, J. Catal. 201 (2001) 275.
[16] R.H. Nibbelke, A.J.L. Nievergeld, J.H.B.J. Hoebink, G.B. Marin, Appl. Catal. B 19 (1998) 245.
[17] J.M.A. Harmsen, J.H.B.J. Hoebink, J.C. Schouten, Stud. Surf. Sci. Catal. 133 (2001) 349.
[18] J.M.A. Harmsen, J.H.B.J. Hoebink, J.C. Schouten, Catal. Lett. 71 (2001) 81.
[19] M. Kolodziejczyk, R.E.R. Colen, M. Berdau, B. Delmon, Surf. Sci. 375 (1997) 235.
[20] I.N. Yakovkin, V.I. Chernyi, A.G. Naumovets, Surf. Sci. 442 (1999) 81.
[21] A. Drewsen, A. Helmersson, M. Skoglundh, B. Andersson, Chem. Eng. Sci. 55 (2000) 4939.
[22] M. Skoglundh, P. Thormählen, E. Fridell, F. Hajbolouri, E. Jobson, Chem. Eng. Sci. 54 (1999) 4559.
[23] P.A. Carlsson, P. Thormählen, M. Skoglundh, H. Persson, E. Fridell, E. Jobson, B. Andersson, Top. Catal. 16/17 (2001) 343.
[24] S. Ljungström, D. Chakarov, J. Bergeld, S. Johansson, B. Kasemo, Top. Catal. 16/17 (2001) 433.
[25] R.N. Miller, R.P. Caren, J.A. Ekchian, US Patent 5,806,305 (1996), to Lockheed Martin Corporation.
[26] A. Naydenov, D. Mehandjiev, Dokl. Akad. Nauk. 46 (1993) 49.
[27] A. Naydenov, R. Stoyanova, D. Mehandjiev, J. Mol. Catal. A. 98 (1995) 9.
[28] A. Naydenov, D. Mehandjiev, Dokl. Akad. Nauk. 50 (1997) 65.
[29] Z. Hao, D. Cheng, Y. Guo, Y. Liang, Appl. Catal. B. 33 (2001) 217.
[30] A. Gervasini, C.L. Bianchi, V. Ragaini, ACS Symp. Ser. 552 (1994) 353.
[31] P. Lööf, B. Kasemo, S. Anderssson, A. Frestad, J. Catal. 130 (1991) 181.
[32] J.R. Andersson, Structure of Metallic Catalysts, Academic Press, London, 1975, p. 296.
[33] V.P. Zhdanov, Elementary Physicochemical Processes on Solid Surfaces, Plenum, New York, 1991, p. 109.
[34] M. Rinnemo, D. Kulginov, S. Johansson, K.L. Wong, V.P. Zhdanov, B. Kasemo, Surf. Sci. 376 (1997) 297.
[35] R.B. Bird, W.E. Stewart, E.N. Lightfoot, Transport Phenomena, J. Wiley and Sons, New York, 1960.
[36] R.D. Hawthorn, AIChE Symp. Ser. 70 (137) (1974) 428.
[37] E. Tronconi, P. Forzatti, AIChE J. 38 (1992) 201.
[38] R. Siegel, J. Howell, Thermal Radiation Heat Transfer, fourth ed., Taylor & Francis, New York, 2002, p. 844.
[39] U. Adler, H. Bauer, A. Cypra, F. Dinkler, P. Künne, J. Röder, Bosch Automotive Handbook, third ed., Robert Bosch GmbH, Stuttgart, 1993, p. 207.
[40] Y.Y. Yeo, L. Vattuone, D.A. King, J. Chem. Phys. 106 (1997) 392.
[41] A. Bourane, D. Bianchi, J. Catal. 218 (2003) 447.
[42] P.-A. Carlsson, M. Skoglundh, P. Thormählen, B. Andersson, Top. Catal. 30/31 (2004) 375.
[43] P. Hunter, S.T. Oyama, Control of Volatile Organic Compound Emissions: Conventional and Emerging Technologies, John Wiley & Sons, New York, 2000, p. 182.
[44] P.W. Atkins, Physical Chemistry, fourth ed., Oxford University Press, Oxford, 1990, p. 944.